PCCP

PAPER

Cite this: *Phys. Chem. Chem. Phys.*, 2017, **19**, 1516

Solvent effects on the triplet–triplet annihilation upconversion of diiodo-Bodipy and perylene†

Qiaohui Zhou,[a] Miaomiao Zhou,[b] Yaxiong Wei,[a] Xiaoguo Zhou,*[ac] Shilin Liu,[ac] Song Zhang*[b] and Bing Zhang[b]

Received 8th October 2016,
Accepted 2nd December 2016

DOI: 10.1039/c6cp06897a

www.rsc.org/pccp

Solvent effects play a very important role in photochemical reactions and energy transfer processes in solution; however, these effects are rarely mentioned in the triplet–triplet annihilation (TTA) upconversion fluorescence experiments. In a typical TTA upconversion system of a photosensitizer of diiodo-Bodipy (**I_2-Bodipy**) and a triplet acceptor of perylene, five common inert solvents, hexane, heptane, toluene, 1,4-dioxane, and dimethyl sulfoxide (DMSO), were used to investigate the solvent effects on the overall quantum yield of upconversion fluorescence. Femtosecond and nanosecond time-resolved transient difference absorption spectra were obtained to study the efficiencies of intersystem crossing (ISC) and triplet–triplet energy transfer (TTET). From the obtained upconversion fluorescence emission spectra, the overall TTA upconversion fluorescence quantum yield was derived. Among the five solvents, the upconversion quantum yield in dioxane is the highest at 19.16%, more than twice that that in toluene (8.75%). For the solvents hexane, heptane, toluene, and dioxane, the yields generally follow the sequences of polarity and viscosity. However, a very low upconversion quantum yield (1.51%) was observed in DMSO although the TTET process and fluorescence quantum yield of perylene in DMSO were almost as efficient as in dioxane. Based on density functional theory calculations, a reasonable explanation for these solvent effects was proposed.

1. Introduction

Since upconversion fluorescence was observed over 50 years ago,[1] it has attracted extensive attention due to its potential applications in photo-dynamic therapy, photovoltaics, and photocatalysis.[2–7] Some traditional methods, including upconversion with two-photon absorption dyes, inorganic crystals and rare earth materials, have been developed to exploit this phenomenon.[8,9] However, the drawbacks of high excitation power, weak absorption of visible light, and low upconversion quantum yield have restricted the application of these methods. Recently, triplet–triplet annihilation (TTA) upconversion has received wide interest due to its overwhelming advantages of intense absorption of solar light and high upconversion quantum yields.[10,11] Moreover, TTA upconversion fluorescence is extremely useful in bioimaging when the prompt fluorescence techniques cannot be applied.[12–14]

The overall TTA upconversion process is shown in Scheme 1, and the excitation mainly involves four steps: intersystem crossing (ISC) from the singlet excited state to the triplet state of the photosensitizer, triplet–triplet energy transfer (TTET) from the triplet sensitizer to the triplet acceptor, TTA of the triplet acceptor and delayed fluorescence (upconversion fluorescence) emission of the excited acceptor. The synthesis of a new triplet photosensitizer with more intense absorption of visible light

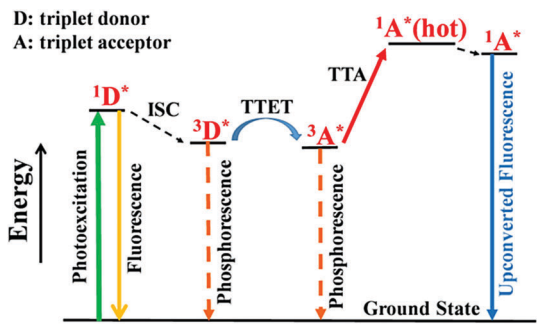

Scheme 1 Jablonski diagram of the overall TTA upconversion process. **I_2-Bodipy** is the triplet donor (photosensitizer) and perylene is the triplet acceptor in the present experiment.

[a] *Hefei National Laboratory for Physical Sciences at the Microscale and Department of Chemical Physics, University of Science and Technology of China, Hefei, Anhui 230026, China. E-mail: xzhou@ustc.edu.cn*
[b] *State Key Laboratory of Magnetic Resonance and Atomic and Molecular Physics, Wuhan Institute of Physics and Mathematics, Chinese Academy of Sciences, Wuhan 430071, China. E-mail: zhangsong@wipm.ac.cn*
[c] *Synergetic Innovation Center of Quantum Information & Quantum Physics, University of Science and Technology of China, Hefei, Anhui 230026, China*

† Electronic supplementary information (ESI) available. See DOI: 10.1039/c6cp06897a

and higher ISC efficiency is most attractive. Some organic compounds, *e.g.* RuBpy, Pt(II) and Ir(III) porphyrin complexes, are often used as triplet photosensitizers because they have a very high ISC efficiency due to the "heavy-atom effect".[15–21] Among these sensitizers, boron-dipyrromethene (Bodipy) derivatives show two major merits: strong absorption in the visible light range and readily modified structures. Many efforts have been made to synthesize new Bodipy-based sensitizers with improved anti-Stokes shifts and upconversion efficiencies.[22–25] Recently, Zhao and co-workers synthesized a series of metal complexes and pure organic triplet photosensitizers, especially Bodipy derivative dyads.[26–29] These sensitizers had not only strong absorption abilities in the near-infrared wavelength range but also had high ISC efficiencies due to the long lifetimes of the triplet states. An upconversion quantum yield of up to 39.9% was reported for a naphthalimide (NI) acetylide-containing Pt(II) complex.[30]

In TTET and TTA processes, a triplet donor must collide with the triplet acceptor in the same solvent cage to generate an encounter. Thus, solvent effects play a very important role in these processes as well as in the characteristics of the triplet sensitizer. However, solvent effects are rarely mentioned in TTA upconversion fluorescence experiments,[11] although they are well studied in photochemical reactions and energy transfer processes.[31–34] Generally, solvents with different polarities and viscosities not only affect the reaction rate, but can also change the resonance wavelength and absorption intensity of molecules.[29,35,36] Because the dipole moments of singlet and triplet states are usually different, the energy gap between them can be influenced by solvents; consequently, different dynamic behaviors should be observed in different solvents.[37–39] Very recently, Yokoyama *et al.* observed the effects of solvent viscosity on the TTA upconversion of platinum octaethylporphyrin and DPA.[40] By changing the temperature and applying a magnetic field, the delayed fluorescence of DPA was found to be dependent on the solvent viscosity. However, the viscosity (or polarity) dependence of absorption and the ISC efficiency of the triplet sensitizer were artificially ignored, and the solvent effects on the prompt fluorescence quantum yield of the annihilator were also not discussed.

In the present work, a typical TTA upconversion system of **I_2-Bodipy** and perylene has been investigated in five separate solvents: hexane, heptane, toluene, 1,4-dioxane and DMSO. All these solvents are chemically inert and have relatively low volatility. Through comparing the dynamic behavior and upconversion efficiency of the system in different solvents, the solvent effects can be clearly observed. As previous experiments have shown,[27] **I_2-Bodipy** in toluene absorbs visible light in the wavelength range of 500 to 550 nm and produces the triplet state with high ISC efficiency due to the heavy atom effect of iodine. The triplet state of a $\sim$50 μs long lifetime supports the role of the triplet donor, and triplet perylene can be formed as the triplet acceptor in the TTET process. TTA upconversion fluorescence was finally observed in the range of 430 to 530 nm with a moderate upconversion efficiency of 7.5%. Although the upconversion spectra and efficiencies have been previously obtained, the dynamic details of the overall process, *e.g.* the ISC efficiency, are still unknown. More importantly, solvent effects have never been investigated in this TTA upconversion system. Therefore, femtosecond and nanosecond transient difference absorption spectra and upconversion spectra were applied to acquire this useful dynamic information. Consequently, the solvent effects on all the involved dynamic processes will be discussed separately.

2. Materials and methods

2.1 Triplet photosensitizers and triplet acceptors of TTA upconversion

Bodipy 1 has strong absorption in the visible light region, and its fluorescence quantum yield is also quite high. Based on its modifiable structure, iodine atoms were attached on the core of the fluorophore, as shown in Scheme 2. The details of the synthetic process were very similar to those in ref. 27. The structure of **I_2-Bodipy** was verified by mass spectrometry and by ^{1}H NMR and ^{13}C NMR spectroscopy. All the precursors were analytically pure and were purchased from Sigma-Aldrich Co. and used without any purification. The solvents were dried and distilled prior to use.

In the present experiment, **I_2-Bodipy** served as both the light-harvesting antenna and the triplet donor. Usually, a triplet acceptor in TTA upconversion should have a high fluorescence quantum yield and lower triplet energy than the donor. Another essential limitation of TTA for the triplet acceptor is that the energy of its S_1 state should be slightly less than twice the T_1 energy. Thus, most triplet acceptors are polycyclic aromatic hydrocarbon compounds; here, perylene was chosen as the triplet acceptor in the TTA upconversion system.

2.2 Experimental setups

The steady-state UV-vis absorption and fluorescence spectra were recorded from 400 to 650 nm (UV-3600, Shimadzu) and from 500 to 680 nm (F-4600, Hitachi), respectively. The structures of all the synthesized chemicals were identified using standard NMR and mass spectra. The ^{1}H NMR spectra were recorded with a 400 MHz spectrophotometer (AVANCE III 400, Bruker); $CDCl_3$ was used as the solvent, and TMS was the standard for which δ = 0.00 ppm. The high-resolution mass spectra (HR-MS) were measured with a MALDI-TOFMS spectrometer (GCT, Micromass UK).

The photochemical behaviors of the present chemical systems were studied using femtosecond and nanosecond time-resolved

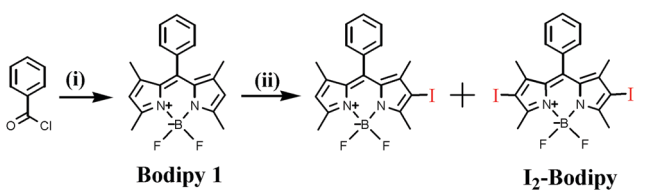

Scheme 2 Synthesis of 2,6-diiodo-1,3,5,7-tetramethyl-8-phenyl-4,4-difluoroboradiazaindacene (**I_2-Bodipy**). (i) N_2 atmosphere, CH_2Cl_2, Et_3N, and $BF_3{\cdot}Et_2O$; (ii) NIS and CH_2Cl_2, 1 h.[27]

transient absorption spectra. The details of femtosecond transient absorption spectra have been described elsewhere;[41] thus, only a brief introduction is provided here. Ti:sapphire in a femtosecond laser system was pumped by the CW second harmonic of a Nd:YVO_4 laser and amplified by a Nd:YLF laser to generate a 35 fs pulse width centered at 800 nm with a maximum energy of 1 mJ per pulse. A fraction of the laser was frequency doubled in a 1 mm thick BBO crystal, and a pulse at 400 nm with an energy of 100 μJ was yielded to pump the NOPA. The output NOPA was set at 532 nm and used as the excitation pulse in the present experiment. The energy was about ~4.5 μJ by attenuation. The NOPA pulse was temporally compressed to obtain the minimum pulse width compatible with the bandwidth. A white light continuum generated by focusing 800 nm on a CaF_2 plate was reflected from the front and back surfaces of a quartz plate to obtain the probe and reference beams. The relative polarization of the pump and probe pulses was maintained as 54.7° for all the measurements. The absorption spectra were detected with a CCD camera equipped with a spectrometer (Princeton, SpectraPro 2500i). The instrumental response function of the system was typically better than 150 fs.

The nanosecond time-resolved transient absorption spectra and dynamics curves were measured based on a home-built laser flash photolysis system.[42,43] The second harmonic (532 nm) of a Q-switched Nd:YAG laser (Lab-170, Spectra Physics, repetition rate of 10 Hz) was used as the excitation light (pulse duration 8 ns, pulse energy ~7 mJ per pulse). An analyzing light from a 500 W xenon lamp and the pulsed excitation laser passed through a flow quartz cuvette perpendicularly. The transient absorption spectra and dynamic curves were measured with a monochromator equipped with a photomultiplier (CR131, Hamamatsu), and the data were recorded with an oscilloscope (TDS3052B, Tektronix).

The upconversion fluorescence spectra were measured using a modified commercial spectrometer. A pump laser of ~20 mW from a stable CW laser (Verdi-V5, 532 nm, Coherent) was used as the excitation light in the TTA upconversion. The fluorescence was dispersed and detected with a triple monochromator system (TriplePro, Acton Research) and a CR131 photomultiplier. In order to reduce self-absorption, the backscattering geometry was applied.[44,45] The normal spectral resolution was ~1.0 cm^{-1}. In the present experiments, the concentrations of **I_2-Bodipy** and perylene were fixed respectively at 5.0×10^{-6} M and 3.0×10^{-4} M in the five selected solvents. All the samples in the nanosecond transient and upconversion experiments were deoxygenated by purging with high-purity argon (99.99%) for at least 20 minutes in advance. Also, the degassing was continued during the measurements to ensure an anaerobic environment.

2.3 Theoretical calculations

The geometries of **I_2-Bodipy** and perylene were optimized with density functional theory (DFT) at the B3LYP/6-31G(d,p) level of theory. Due to the heavy-atom effect of iodine, the LanL2DZ basic set was introduced into the DFT calculations of the photosensitizer, **I_2-Bodipy**. The spin density surface of **I_2-Bodipy** was analyzed at the same level of theory. Based on the optimized structure of the ground state, time-dependent DFT (TDDFT) with the PCM model was used to calculate the excitation energies of the lowest singlet S_1 and triplet T_1 states of **I_2-Bodipy** and perylene in different solvents. All the calculations were performed with the Gaussian 09W program package.[46]

3. Results and discussion

3.1 Steady-state UV-visible absorption and fluorescence spectra

Fig. 1(a) shows the steady-state UV-visible absorption spectra of **I_2-Bodipy** in the five solvents. The maximum absorption is located at 537 nm, along with a shoulder band at ~504 nm. In addition to slight red-shifts, the intensities of the maximum absorption in different solvents obviously changed. The molar extinction coefficient ε varies from 1.24×10^5 M^{-1} cm^{-1} in heptane to 6.97×10^4 M^{-1} cm^{-1} in DMSO. The fluorescence emission spectra of **I_2-Bodipy** upon photoexcitation at 532 nm are shown in Fig. 1(b). Similar to the UV-vis absorption spectra in Fig. 1(a), a slight red-shift can be observed in the range of 552 to 561 nm, and the maximum intensity shows a 4.7-fold enhancement from DMSO to heptane.

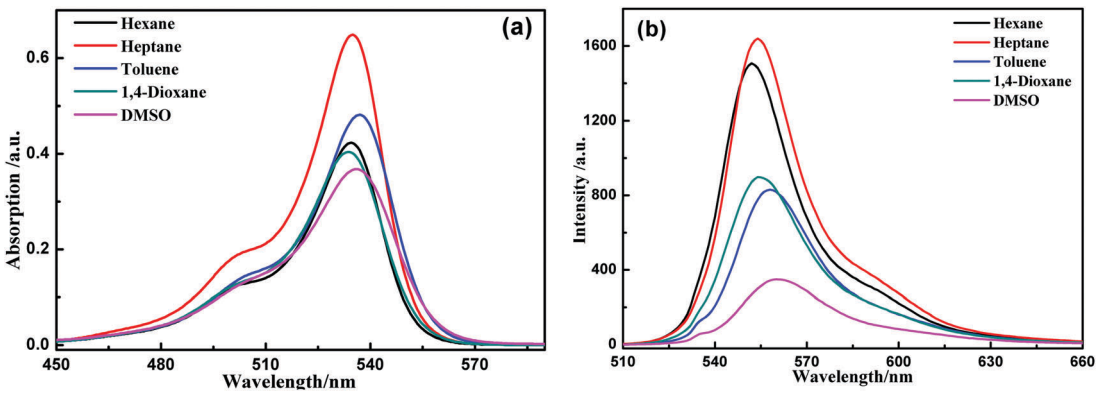

Fig. 1 UV-vis absorption (a) and fluorescence emission (b) spectra of **I_2-Bodipy** in different solvents ($c = 5 \times 10^{-6}$ M).

Table 1 Photophysical parameters of **I_2-Bodipy**

Solvent	λ_{abs} (nm)	ε^a ($\times 10^4$ M^{-1} cm^{-1})	λ_{em} (nm)	$\Phi_F{}^b$ (%)
Hexane	534	8.18	552	4.86 ± 0.05
Heptane	535	12.4	554	3.14 ± 0.05
Toluene	537	8.6	558	3.01 ± 0.08
Dioxane	534	8.0	555	3.27 ± 0.08
DMSO	536	7.0	561	1.12 ± 0.09

[a] Molar absorption coefficient. [b] Prompt fluorescence quantum yield with photoexcitation at 532 nm.

Table 1 summarizes the absorption and emission wavelengths, molar absorption coefficients and fluorescence quantum yields. Without substitution of iodine atoms, Φ_F of **Bodipy 1** was 0.712, while the Φ_F of **I_2-Bodipy** dramatically decreased to a very low percentage. As direct photoexcitation to the triplet state (T_1) is transition-forbidden, the only way to form the T_1 state to compete with the fluorescence emission is *via* ISC. As shown in the Jablonski diagram in Scheme 1, the decreased Φ_F of **I_2-Bodipy** indicates a greater population of the triplet state.

3.2 Femtosecond transient difference absorption spectra

Femtosecond transient difference absorption spectra were measured to characterize the initial photophysical processes of the photosensitizer, *e.g.* the lifetime of the singlet excited state and the ISC rate from S_1 to T_1. Fig. 2(a–e) show the recorded femtosecond transient difference absorption spectra of **I_2-Bodipy** in the five solvents upon photoexcitation at 532 nm. The delay time was gradually changed from 40 fs to 900 ps. One negative

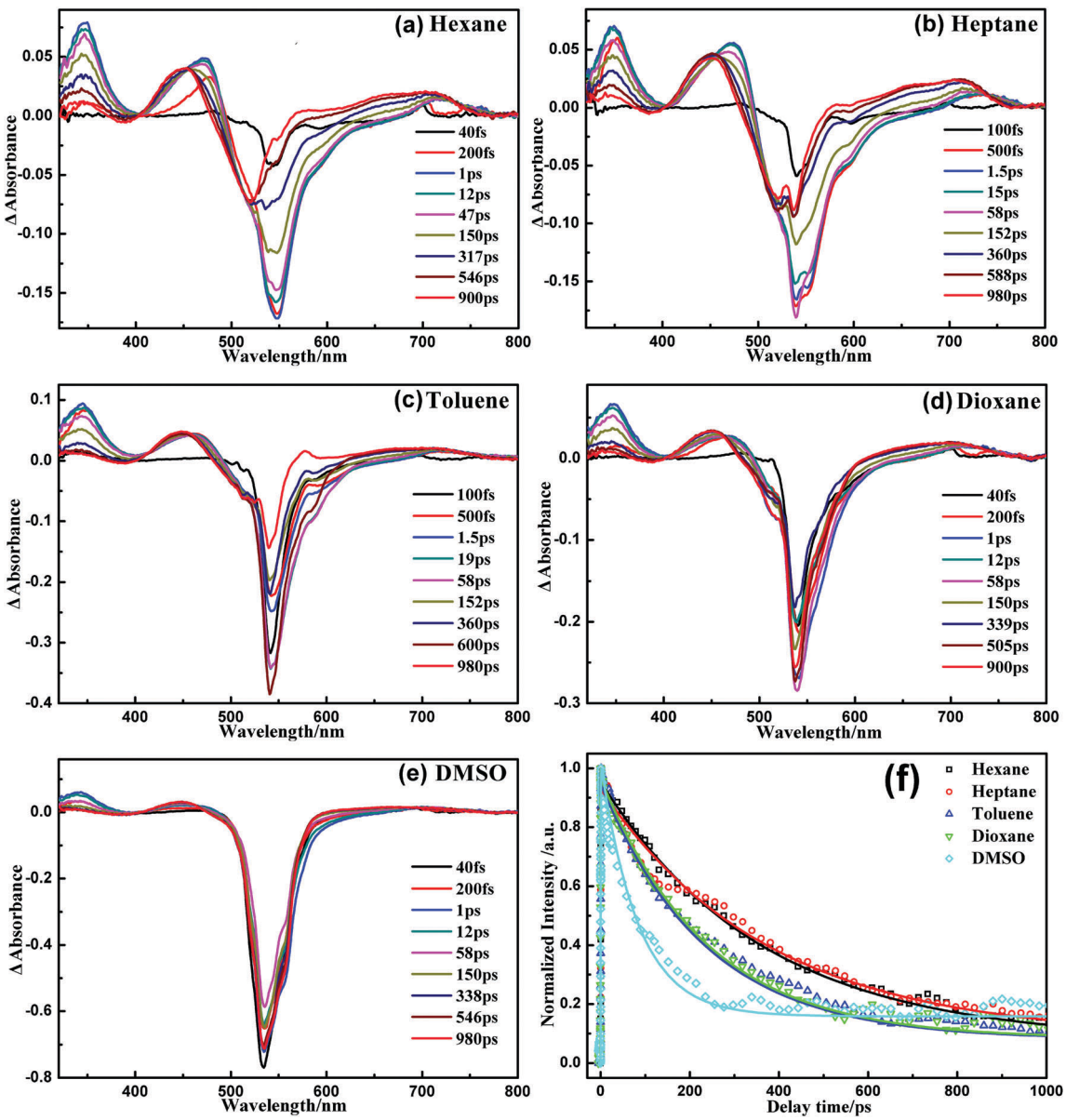

Fig. 2 Femtosecond time-resolved transient difference absorption spectra of **I_2-Bodipy** in (a) hexane, (b) heptane, (c) toluene, (d) dioxane, (e) DMSO. (f) The experimental (dotted lines) and fitted (solid lines) are normalized decay curves of the absorption band at 346 nm (λ_{ex} = 532 nm, $c = 1 \times 10^{-5}$ M).

band (~540 nm) and three positive bands (346, 471 and 716 nm) are present in all the spectra.

Taking the spectra in hexane of Fig. 2(a) as an example, the strongest negative band at 540 nm is assigned to stimulated emission and/or ground bleaching. From the initial 200 fs to 47 ps, the position and intensity of the band do not essentially change. The slight blue-shift is due to the overlapping of the adjacent broad band of 600 to 700 nm (positive peak). The band at 346 nm is a typical positive peak, and its intensity monotonously decays with the delay time. Thus, the band can be attributed to the absorption of the S_1 state, and its decay mainly corresponds to the $S_1 \rightarrow S_0$ process. Interestingly, the band at 471 nm with moderate intensity quickly increased to the maximum in the first picosecond, then slowly decayed and gradually blue-shifted to 450 nm. The isoabsorptive point is located at 453 nm, and its intensity remained strong during the entire present delay time range. Therefore, an ISC process to produce the triplet state is expected, and the absorption of the latter contributes the band. With increasing delay time, the weak peak at ~700 nm shows an overall trend of growing and broadening. From 1 ps on, the intensity at 716 nm monotonously increases, and the absorption is gradually blue-shifted. This long delay timescale indicates that a triplet excited state is generated, which is consistent with the above conclusion. Thus, the absorption of the triplet state T_1 is believed to contribute the bands at 450 and 716 nm. Actually, the following nanosecond transient difference spectra also verify the spectral assignment.

As shown in Fig. 2(a–e), the peak patterns remain almost the same in different solvents; however, the lifetimes of the excited states of **I_2-Bodipy** obviously change from hexane to DMSO. As shown in Fig. 2(f), the intensity at 346 nm was normalized to compare and obtain the lifetime of the S_1 state. With increasing solvent polarity and viscosity, the decay rate gradually increases.

Table 2 The decay dynamic data of $^1I_2$-Bodipy* in five solvents

Solvent	Polarity[a]	τ_1 (ps)	τ_2 (ps)
Hexane	0.06	1.90	362
Heptane	0.2	1.05	375
Toluene	2.4	0.62	235
Dioxane	4.8	0.45	234
DMSO	7.2	0.36	83

[a] The relative dielectric constant ε.

By fitting all the curves with a triple-exponential function, all the dynamic parameters of the decay process of the S_1 state were obtained. Three dynamic decay processes were taken into account with three typical time components, τ_1, τ_2 and τ_3, respectively. The first (τ_1) was the natural lifetime of the S_1 state (here, it mainly corresponds to the internal conversion of $S_1 \rightarrow S_0$), the second (τ_2) was the ISC time to form the triplet state T_1, and the third (τ_3) was other slow decays involving collisions and unknown processes. Because we are not concerned with the slowest process of τ_3 in the present ultrafast experiment, Table 2 only summarizes the data of τ_1 and τ_2. Usually, internal conversion has a very fast decay (~10^{-12} s), and τ_1 indeed decreases from 1.9 ps to 0.36 ps with the polarity order from hexane to DMSO. In the same sequence, τ_2 of the ISC process is reduced from 362 ps to 83 ps.

The energy gap ΔE_{ST} between the S_1 and T_1 states is the essential element of the rate of ISC. However, the excitation energy of the T_1 state of **I_2-Bodipy** could not be easily obtained due to a lack of phosphorescence at either room temperature or low temperature; thus, TD-DFT calculations were performed to estimate the excitation energies of the low-lying electronic states. Fig. 3 shows the calculated excitation energies of $S_0 \rightarrow S_1$ and $S_0 \rightarrow T_1$ of **I_2-Bodipy**, where the energy of the ground state in DMSO is set as zero. As noted in Fig. 3, both the $S_0 \rightarrow S_1$ and $S_0 \rightarrow T_1$ excitation energies were almost unchanged (2.65 to 2.67 eV and 1.52 to 1.53 eV) from hexane to dioxane. It is interesting that the S_1 energy dramatically decreases to 2.53 eV in DMSO, which has the highest polarity, but the $S_0 \rightarrow T_1$ energy increases only slightly from 1.52 eV in hexane to 1.55 eV in DMSO. Thus, ISC from S_1 to T_1 of **I_2-Bodipy** in DMSO should be the most favorable because it has the lowest energy gap, ΔE_{ST}, compared with the other solvents. This conclusion is in excellent agreement with the experimental data shown in Table 2.

3.3 Quenching process of triplet I_2-Bodipy by perylene

Upon photoexcitation at 532 nm, the triplet photosensitizer, $^3I_2$-Bodipy*, is produced and quenched by triplet acceptors and collisions in solution. Nanosecond transient difference absorption spectra were used to study this quenching process in the five solvents. Fig. 4 shows the transient difference absorption spectra of **I_2-Bodipy** in toluene with photoexcitation at 532 nm; the spectra in the other solvents are summarized in the ESI.† All the spectra have very similar profiles in the five solvents.

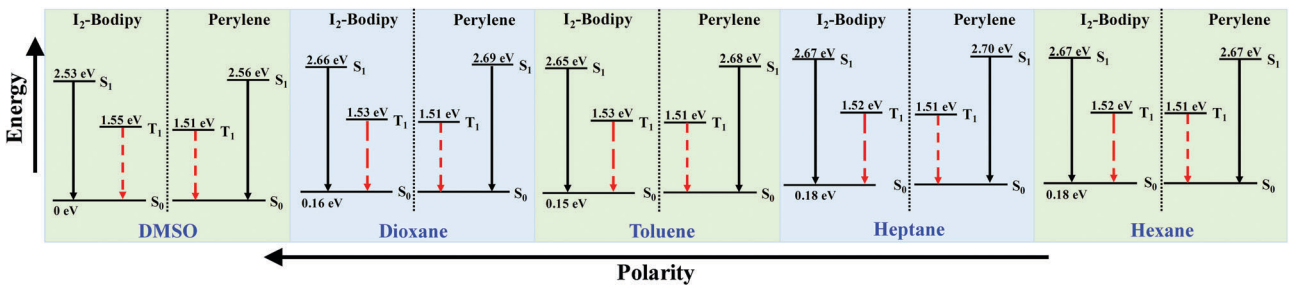

Fig. 3 The excitation energies of the low-lying electronic states of **I_2-Bodipy** and perylene in different solvents, calculated at the TD-B3LYP/6-31G(d,p) level of theory.

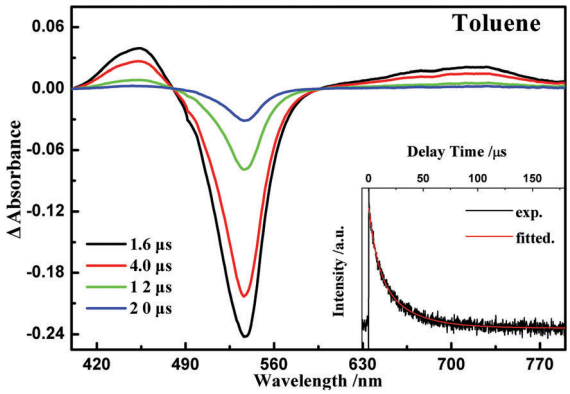

Fig. 4 Nanosecond transient difference absorption spectra of **I_2-Bodipy** in toluene under photoexcitation at 532 nm ($c = 1 \times 10^{-5}$ M); the experimental and fitted decay curves at 710 nm are plotted in the inset panel.

The bleaching band at 537 nm is due to the depletion of the ground state of **I_2-Bodipy**. Two other positive bands at 443 nm and 710 nm are attributed to absorption of the triplet state T_1 of **I_2-Bodipy**. The assignment was confirmed by an additional aerated experiment.[27] The intensities of the three bands show almost the same variations with delay time.

The concentration of the photosensitizer always plays a key role in the lifetime of the triplet state; an overly high concentration is expected to lead to serious self-quenching. Thus, the concentration of **I_2-Bodipy** in the present experiment was maintained at 1.0×10^{-5} M to balance the better signal-to-noise ratio and the lifetime measurements. Because the three bands have very similar decay rates, only the dynamic curve of 710 nm is shown in the inset panel of Fig. 4. In toluene, a lifetime (τ_0) of 50.12 μs was obtained for the triplet state T_1 of $^3I_2$-Bodipy* by fitting the curve. With increasing solvent viscosity, the T_1 lifetime of $^3I_2$-Bodipy* increased from 13.0 μs in hexane to 95.8 μs in DMSO, as shown in Fig. 5(a). The trend is consistent with the calculated energies of the T_1 state in different solvents, as shown in Fig. 3.

This long lifetime of $^3I_2$-Bodipy* provides a high possibility of TTET between $^3I_2$-Bodipy* and the triplet acceptor when the latter is added to the solution. The TTET process between $^3I_2$-Bodipy* and perylene can be briefly described by the following formula (1). In the present experiment, all the absorption bands in Fig. 4 were indeed dramatically quenched in the presence of perylene (as the triplet acceptor). The observed quenching rate $k_{obs} = 1/\tau$ of $^3I_2$-Bodipy* was obtained by fitting its decay curve at 710 nm. Fig. 5(b) shows the relationships between $1/\tau$ and the concentration of perylene in different solvents. Using the Stern–Volmer eqn (2), the bimolecular quenching rate constant, k_q, was obtained by linear-fitting the relationship of Fig. 5(b).

$$^3I_2\text{-Bodipy}^*(T_1) + \text{perylene}(S_0) \rightarrow {}^1I_2\text{-Bodipy}(S_0) + {}^3\text{perylene}^*(T_1) \quad (1)$$

$$k_{obs} = 1/\tau = 1/\tau_0 + k_q \cdot [\text{perylene}] \quad (2)$$

where τ_0 represents the lifetime in the absence of perylene. Table 3 lists the fitted $1/\tau_0$ and bimolecular quenching rate constants k_q in the five solvents, as well as the diffusion rates $k_{diffuse}$. $k_{diffuse}$ can be determined as $8k_BT/(3\eta)$ as the upper limit of k_q, where η is the viscosity of the solvent. Obviously, all k_q values are close to $k_{diffuse}$, indicating that the TTET between $^3I_2$-Bodipy* and perylene is mainly a diffusion-controlled dynamic process. In addition, both k_q and $k_{diffuse}$ follow the same sequence as $1/\tau_0$ in the five solvents.

As suggested in the Dexter mechanism, the exchanged electrons should occupy the orbital of the other party, and the energy transfer rate is proportional to the spectral integral overlap at the short collision distance. Thus, the diffusion rates in solvents of various viscosities may be the rate-controlling factor in the overall TTA upconversion process.[11] In addition, a suitable triplet acceptor should have lower energy than the triplet donor. As expected, the triplet energy of $^3I_2$-Bodipy*(T_1) varies with the solvent; the T_1 energy of perylene must be checked carefully in different solvents. At the B3LYP/6-31G(d,p) level of theory, the energy of ^{3}perylene*(T_1) was determined to be 1.51 eV and was almost unchanged in all five solvents (in Fig. 3), which agrees with previous data (1.53 eV in toluene).[27] Compared with the energy of $^3I_2$-Bodipy*(T_1), perylene is an

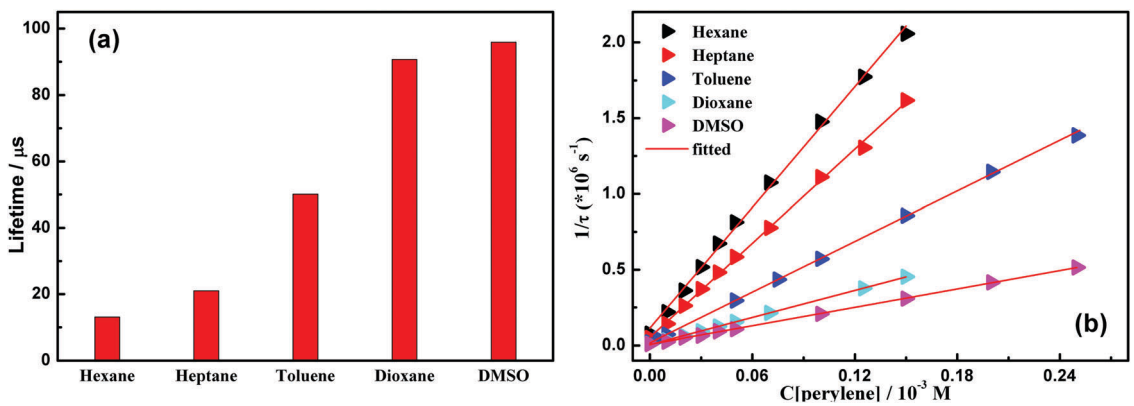

Fig. 5 (a) Lifetimes of the triplet state T_1 of $^3I_2$-Bodipy* in five solvents; (b) Stern–Volmer plots generated from the T_1 quenching of **I_2-Bodipy** in the presence of perylene in the five solvents ([**I_2-Bodipy**] = 5.0×10^{-6} M, λ_{ex} = 532 nm).

Table 3 Bimolecular reaction rate constants k_q of $^3I_2$-Bodipy* quenched by perylene, as well as ΔE_{TTET} between $^3I_2$-Bodipy* and ^{3}perylene* in five solvents

Solvent	H (cp)	$1/\tau_0$ ($\times 10^4$ s^{-1})	k_q ($\times 10^9$ M^{-1} s^{-1})	$k_{diffuse}$ ($\times 10^9$ M^{-1} s^{-1})	ΔE_{TTET} (eV)	K_{SV} ($\times 10^5$ M^{-1})
Hexane	0.33	7.64	13.30	19.67	0.014	1.74
Heptane	0.41	4.77	10.33	15.83	0.014	2.17
Toluene	0.59	1.99	5.57	11.0	0.017	2.79
Dioxane	1.54	1.10	2.98	4.21	0.016	2.70
DMSO	2.24	1.04	2.03	2.89	0.032	1.94

excellent triplet acceptor due to its slightly lower energy than the triplet donor. As shown in Table 3, ΔE_{TTET} slightly increased from 0.01 eV in hexane to 0.03 eV in DMSO; all of the values are very small. Therefore, viscosity should play a larger role in the TTET process, and the TTET rates are expected to decrease with increasing solvent viscosity. The present experimental results are indeed consistent with the theoretical predictions.

Generally, K_{SV} is a reliable criterion to evaluate the quenching ability of a triplet sensitizer by an acceptor; it is defined as $K_{SV} = k_q \cdot \tau_0$. As shown in Table 3, K_{SV} does not directly follow the order of the viscosity and polarity of the solvents. The maximal value of K_{SV} is 2.79×10^5 M^{-1} in toluene, nearly $\sim$1.4 times the K_{SV} in DMSO. This is a potential reason why the previous investigation[27] invariably used toluene as a solvent in TTA upconversion. Additionally, the TTET quantum yields, $\Phi_{TTET} = k_q \cdot [\text{perylene}]/(1/\tau_0 + k_q \cdot [\text{perylene}])$, are expected to follow the same sequence as K_{SV}. When the concentration of perylene is increased to 7×10^{-5} M, Φ_{TTET} is close to unity ($k_q \cdot [\text{perylene}] = 20/\tau_0$) in dioxane. In the following TTA upconversion measurements, the concentration of perylene was 3×10^{-4} M; thus, the TTET quantum yield was near unity in all the solvents.

3.4 TTA upconversion fluorescence spectra of ^{3}perylene*

When triplet perylene is produced, upconversion fluorescence can be observed due to the TTA process of ^{3}perylene*.[48] In the present experiment, white upconversion fluorescence (in Fig. 6(a)) could be observed under photoexcitation of a CW 532 nm laser ($\sim$20 mW, power density 630 mW cm^{-2}); the intensities of fluorescence were remarkably different in the five solvents. Because this upconversion fluorescence cannot appear upon photoexcitation of **I_2-Bodipy** or perylene alone, it can be attributed to upconverted delayed fluorescence rather than prompt fluorescence. Fig. 6(b) shows the dispersed upconversion fluorescence spectra in the five solvents. Obviously, the observed fluorescence is a mixture of the yellowish-green fluorescence of **I_2-Bodipy** itself ($\sim$552 nm) and the blue upconversion fluorescence of perylene (400 to 500 nm).

As shown in Fig. 6(a), the brightest delay fluorescence was emitted in dioxane, while the weakest was emitted in DMSO. In hexane and heptane, the upconversion fluorescence is weaker than the prompt fluorescence of the photosensitizer (**I_2-Bodipy**), although it can be clearly distinguished in Fig. 6(a). Similar to the previous experiment in toluene,[27] upconversion fluorescence was also observed in a wavelength range of 440 to 480 nm. Using the fluorescence of **I_2-Bodipy** as the standard (Φ_{std} = 2.7% in ACN), the upconversion quantum yields (Φ_{UC}) could be determined with eqn (3),

$$\Phi_{UC} = 2 \cdot \Phi_{std} \cdot \left(\frac{A_{std}}{A_{sam}}\right) \cdot \left(\frac{I_{sam}}{I_{std}}\right) \cdot \left(\frac{\eta_{sam}}{\eta_{std}}\right)^2 \quad (3)$$

where A, I, and η are the absorbance intensities, integrated luminescence intensities, and refractive indices of the solvents used for the standard and samples. The equation is multiplied by a factor of 2 to bring the maximum quantum yield to unity.[12] Thus, the upconversion quantum yields Φ_{UC} of the present system were determined to be 5.77% in hexane, 5.59% in heptane, 8.44% in toluene, 19.16% in dioxane and 1.51% in DMSO. The present yield in toluene is slightly higher than the previously reported value (7.5%).[27] Table 4 summarizes the quantum yields of the TTA upconversion fluorescence under irradiation at 532 nm and the prompt fluorescence of perylene alone.

It is well known that delayed fluorescence intensity shows a quadratic dependence on excitation power at low intensities and shifts to a linear dependence at higher intensities.[11] In the

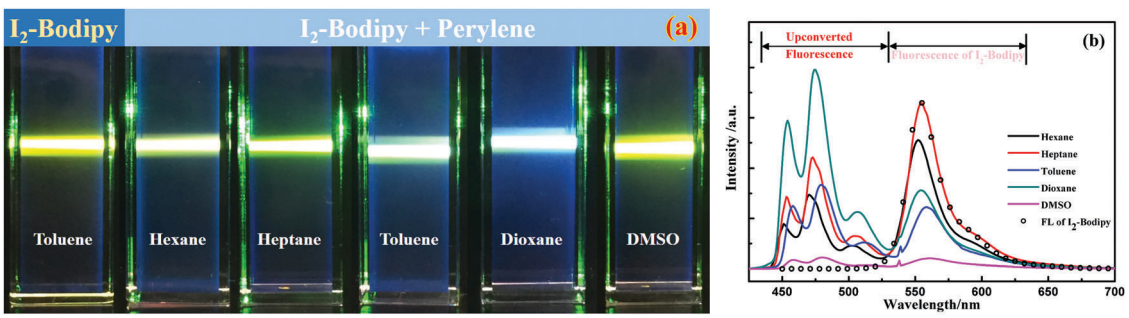

Fig. 6 (a) Images of the upconversion fluorescence in different solvents; (b) TTA upconversion fluorescence spectra of **I_2-Bodipy** and perylene, where the curve denoted by hollow circles is the prompt fluorescence of **I_2-Bodipy** alone in heptane under excitation at 532 nm. [**I_2-Bodipy**] = 5×10^{-6} M, and [perylene] = 3×10^{-4} M.

Table 4 Quantum yields of the TTA upconversion fluorescence of ^{3}perylene* in the five solvents under photoexcitation at 532 nm, as well as the prompt fluorescence yield of perylene alone

Solvent	ΔE_{TTA} [a] (eV)	$\Delta E_{2T_1-T_2}$ [b] (eV)	Φ_{Py} [c] (%)	Φ_{UC} (%)
Hexane	0.31	0.001	44.06 ± 0.04	5.77 ± 0.03
Heptane	0.32	0.001	53.32 ± 0.02	5.59 ± 0.02
Toluene	0.34	0.002	84.81 ± 0.01	8.44 ± 0.05
Dioxane	0.33	0.002	96.78 ± 0.02	19.16 ± 0.02
DMSO	0.47	0.011	78.78 ± 0.02	1.51 ± 0.06

[a] Energy difference of perylene calculated as $\Delta E_{TTA} = 2{\cdot}E(T_1) - E(S_1)$. [b] Energy difference $\Delta E_{2T_1-T_2} = 2{\cdot}E(T_1) - E(T_2)$, where $E(T_1)$ and $E(T_2)$ are the energies of the first and second triplet states of perylene. [c] Prompt fluorescence quantum yield of perylene.

previous experiment of Wu *et al.*,[48] a linear relationship between upconverted fluorescence intensity and excitation power density was observed from 14.2 to 237.8 mW cm^{-2}. Thus, the maximum Φ_{UC} for the present TTA upconversion system has not yet been reached because Φ_{UC} may linearly increase with excitation power under the threshold I_{th}.[11] An additional experiment was performed to determine the threshold power density, as shown in Fig. 7, where the delayed fluorescence intensity was plotted with the excitation power density. A change of dependence was observed from the quadratic function to the linear relationship. The threshold I_{th} was determined as ~259 mW cm^{-2} as the turning point in Fig. 7. In the present TTA upconversion experiment, the excitation power density is higher than I_{th}; hence, the Φ_{UC} value in Table 4 is slightly higher than the previously reported data.[27]

It is very interesting that a high quantum yield (Φ_{UC} = 19.16%) was obtained in dioxane, even higher than the maximal upconversion quantum yield (11.1%) predicted from the spin-statistic law in the TTA process. This exceptional yield is not unique;[47] higher Φ_{UC} values of 24.3% and 39.9% have been observed for a naphthalimide (NI) acetylide-containing Pt(II) complex.[30,35] Ref. 12 and 47 provide a probable explanation that both the quintet and triplet encounter complexes contribute to the formation of the singlets of the annihilator. It is especially noteworthy that among the five solvents, Φ_{UC} in DMSO is exceptionally low (1.51%), although both the quantum yields, Φ_{ISC} and Φ_{TTET}, in DMSO as well as in the other solvents are close to unity.

As indicated in Scheme 1, Φ_{UC} can be determined according to the following eqn (4):

$$\Phi_{UC} = \Phi_{ISC}{\cdot}\Phi_{TTET}{\cdot}\Phi_{TTA}{\cdot}\Phi_{Py} \quad (4)$$

where Φ_{ISC} is the quantum yield of ISC from ^{1}I$_2$-Bodipy*(S$_1$) to ^{3}I$_2$-Bodipy*(T$_1$) and Φ_{Py} is the fluorescence quantum yield of perylene upon excitation. Using the fluorescence yield Φ_F of ^{1}I$_2$-Bodipy*(S$_1$) in Table 1, Φ_{ISC} can be calculated by $\Phi_{ISC} = 1 - \Phi_F$ as 0.95 in hexane to 0.99 in DMSO. Moreover, Φ_{Py} shows moderate dependence on the polarity of the solvent, as shown in Table 4. Fig. 8 shows the fluorescence emission spectra of perylene alone under photoexcitation at 390 nm. The maximal Φ_{Py} value is obtained in dioxane (96.78%), while it is moderate in DMSO (78.78%).

In general, the bottlenecks limiting the overall TTA upconversion efficiency are the TTET and TTA processes. As mentioned above, the quantum yields Φ_{TTET} are close to unity in all the solvents. Moreover, a slight difference is observed in the fluorescence quantum yields of perylene in dioxane and DMSO, as shown in Table 4. Thus, the dramatic difference of Φ_{UC} in dioxane and DMSO originates from the TTA process. In general, the TTA process proceeds according to the Dexter exchange mechanism; the solvent viscosity plays a key role. The present experimental conclusions indicate that the energy gap ΔE_{TTA} between the singlet state and double the triplet state, $\Delta E_{TTA} = 2{\cdot}E(T_1) - E(S_1)$, also plays an important role in addition to the diffusion rate in the TTA process. As V. Gray *et al.* suggested,[49] "ΔE_{TTA} ideally is positive but close to zero for a good annihilator in a TTA upconversion system". ΔE_{TTA} of perylene was calculated at the TD-B3LYP/6-31G(d,p) level of theory and is listed in Table 4 as well. In DMSO, ΔE_{TTA} is apparently larger than in the other solvents. Thus, the remarkable increase of ΔE_{TTA} in DMSO is thought to be a key reason for the low TTA upconversion quantum yield in DMSO. In addition, as Schmidt and Castellano recently pointed out,[50] the TTA yield of a singlet can be reduced when the energy of the second triplet state, T_2, is lower than the

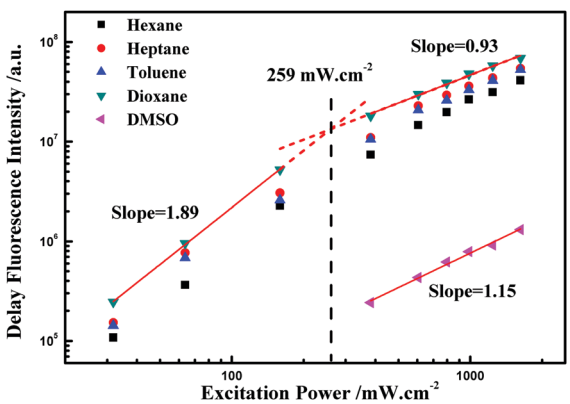

Fig. 7 Normalized integrated delayed fluorescence intensity plotted as a function of light power, where [**I$_2$-Bodipy**] = 5 × 10^{-6} M and [perylene] = 3 × 10^{-4} M.

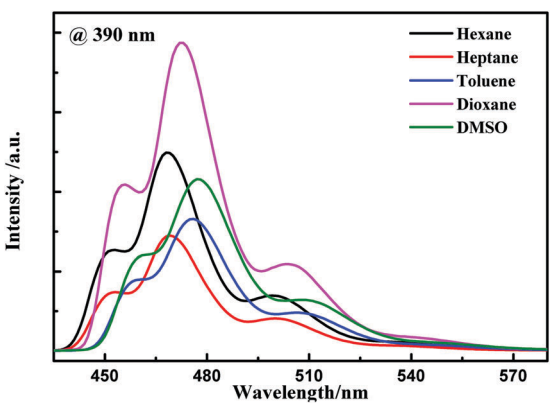

Fig. 8 Fluorescence emission spectra of perylene alone in the five solvents under photoexcitation at 390 nm. c = 3 × 10^{-4} M.

twice the T_1 energy. As shown in Table 4, the energy differences, $\Delta E = 2 \times T_1 - T_2$, apparently increased from near zero to 0.011 eV in DMSO. This is another important reason for this low TTA yield in DMSO. Furthermore, the distance between the two triplets in the annihilator encounter complex is also certainly affected by the polarity and viscosity of the solvent. Therefore, the solvent effects on the TTA yield are considerable; more accurate theoretical and experimental studies are ongoing.

4. Summary and conclusions

It is well known that solvent effects play a very important role in photochemical reactions and energy transfer processes in solution; however, these effects are rarely mentioned in TTA upconversion fluorescence experiments. In a TTA upconversion system of **I_2-Bodipy** (as the triplet photosensitizer) and perylene (as the triplet acceptor), five common inert solvents, hexane, heptane, toluene, 1,4-dioxane and dimethyl sulfoxide (DMSO), were used to investigate solvent effects on the overall quantum yield of upconversion fluorescence.

In the femtosecond time-resolved transient difference absorption spectrum of **I_2-Bodipy**, three positive peaks were observed. The bands at 450 and 716 nm are attributed to absorption of the triplet state T_1, and the peak at 346 nm is attributed to the absorption of the S_1 state. By fitting the decay curves at 346 nm, the lifetime of the S_1 state and the ISC rates from S_1 to T_1 were obtained. Among the five solvents, the lifetime of the S_1 state decreases from 1.9 ps to 0.36 ps with the polarity order from hexane to DMSO. Similarly, the ISC rate increased in the same order, which agrees very well with the calculated energy gap ΔE_{ST} between the S_1 and T_1 states.

When the triplet $^3I_2$-Bodipy* is produced, it can be quickly quenched by triplet acceptors and collisions in solution. From nanosecond transient difference absorption spectra, the lifetime of $^3I_2$-Bodipy* was derived in the absence of perylene. With increasing viscosity of the solvent, the lifetime is prolonged from 13.0 μs in hexane to 95.8 μs in DMSO. This long lifetime of $^3I_2$-Bodipy* provides a high possibility of TTET between $^3I_2$-Bodipy* and perylene when the latter exists in the solution. The bimolecular quenching rate constants k_q were obtained by linear-fitting the Stern–Volmer relationship in the five solvents; the values gradually decreased with increasing solvent viscosity. Additionally, all of the k_q values were close to the diffusion rate $k_{diffuse}$, indicating that the TTET process is indeed a diffusion-controlled dynamic process.

From the TTET process on, triplet perylene was formed, and upconversion fluorescence was then emitted *via* the TTA process. By recording the upconversion fluorescence emission spectra, the overall TTA upconversion fluorescence quantum yield was obtained. Among the five solvents, the upconversion quantum yield in dioxane is the highest at 19.16%. Moderate yields of 8.75% in toluene, 5.77% in hexane and 5.59% in heptane were obtained. For the solvents hexane, heptane, toluene and dioxane, the yields generally follow the sequence of viscosity. To our surprise, a very low upconversion quantum yield of 1.51% was observed in DMSO. Although the key role in the TTA process is generally thought to be diffusion by the Dexter mechanism, the present experimental conclusions indicate that the energy gap ΔE_{TTA} between the singlet state and double the triplet state, $\Delta E_{TTA} = 2{\cdot}E(T_1) - E(S_1)$, also plays an important role. In addition, as the energy differences, $\Delta E = 2 \times T_1 - T_2$, apparently increased from near zero to 0.011 eV in DMSO, the TTA yield of the singlets is naturally reduced to result in a low TTA yield.

In summary, obvious solvent effects have been observed in the TTA upconversion system of **I_2-Bodipy** and perylene under photoexcitation at 532 nm. Although toluene is the most popular solvent in similar TTA systems, it is not the best solvent in the present system for TTA upconversion efficiency. Therefore, choosing a more suitable solvent can efficiently improve upconversion quantum yield, and solvent effects are an important factor, although they have previously been ignored.

Acknowledgements

This work was supported by the National Key Basic Research Foundation (Grant No. 2013CB834602 and 2013CB922202) and the National Natural Science Foundation of China (Grant No. 21373194, 21573210 and 11674355). The quantum chemical calculations in this study were performed on the supercomputing system in the Supercomputing Center of the University of Science and Technology of China. Some experimental instruments were supported by the Ministry of Science and Technology of China (No. 2012YQ220113) as well.

References

1 T. A. Joyce, *Analyst*, 1965, **90**, 1–8.
2 B. C. O'Regan, K. Walley, M. Juozapavicius, A. Anderson, F. Matar, T. Ghaddar, S. M. Zakeeruddin, C. Klein and J. R. Durrant, *J. Am. Chem. Soc.*, 2009, **131**, 3541–3548.
3 T. Lazarides, T. M. McCormick, K. C. Wilson, S. Lee, D. W. McCamant and R. Eisenberg, *J. Am. Chem. Soc.*, 2011, **133**, 350–364.
4 D. P. Hari, T. Hering and B. König, *Org. Lett.*, 2012, **14**, 5334–5337.
5 A. Gorman, J. Killoran, C. O'Shea, T. Kenna, W. M. Gallagher and D. F. O'Shea, *J. Am. Chem. Soc.*, 2004, **126**, 10619–10631.
6 S. Duman, Y. Cakmak, S. Kolemen, E. U. Akkaya and Y. Dede, *J. Org. Chem.*, 2012, **77**, 4516–4527.
7 M. A. Baldo, C. Adachi and S. R. Forrest, *Phys. Rev. B: Condens. Matter Mater. Phys.*, 2000, **62**, 10967–10977.
8 P. Zhang, C. Shao, Z. Zhang, M. Zhang, J. Mu, Z. Guo and Y. Liu, *Nanoscale*, 2011, **3**, 3357–3363.
9 M. Haase and H. Schäfer, *Angew. Chem., Int. Ed.*, 2011, **50**, 5808–5829.
10 V. Gray, D. Dzebo, M. Abrahamsson, B. Albinsson and K. Moth-Poulsen, *Phys. Chem. Chem. Phys.*, 2014, **16**, 10345–10352.

11 A. Monguzzi, J. Mézyk, F. Scotognella, R. Tubino and F. Meinardi, *Phys. Rev. B: Condens. Matter Mater. Phys.*, 2008, **78**, 2–6.
12 T. N. Singh-Rachford and F. N. Castellano, *Coord. Chem. Rev.*, 2010, **254**, 2560–2573.
13 V. Gray, K. Börjesson, D. Dzebo, M. Abrahamsson, B. Albinsson and K. Moth-Poulsen, *J. Phys. Chem. C*, 2016, **120**, 19018–19026.
14 P. Ceroni, *Chem. – Eur. J.*, 2011, **17**, 9560–9564.
15 D. V. Kozlov and F. N. Castellano, *Chem. Commun.*, 2004, 2860–2861.
16 W. Wu, S. Ji, W. Wu, J. Shao, H. Guo, T. D. James and J. Zhao, *Chem. – Eur. J.*, 2012, **18**, 4953–4964.
17 T. N. Singh-Rachford and F. N. Castellano, *J. Phys. Chem. A*, 2008, **112**, 3550–3556.
18 W. Zhao and F. N. Castellano, *J. Phys. Chem. A*, 2006, **110**, 11440–11445.
19 T. N. Singh-Rachford and F. N. Castellano, *J. Phys. Chem. A*, 2009, **113**, 5912–5917.
20 H. C. Chen, C. Y. Hung, K. H. Wang, H. L. Chen, W. S. Fann, F. C. Chien, P. Chen, T. J. Chow, C. P. Hsu and S.-S. Sun, *Chem. Commun.*, 2009, 4064–4066.
21 Y. Y. Cheng, B. Fückel, T. Khoury, R. G. C. R. Clady, N. J. Ekins-Daukes, M. J. Crossley and T. W. Schmidt, *J. Phys. Chem. A*, 2011, **115**, 1047–1053.
22 T. Yogo, Y. Urano, Y. Ishitsuka, F. Maniwa and T. Nagano, *J. Am. Chem. Soc.*, 2005, **127**, 12162–12163.
23 G. Ulrich, R. Ziessel and A. Harriman, *Angew. Chem., Int. Ed.*, 2008, **47**, 1184–1201.
24 A. Loudet and K. Burgess, *Chem. Rev.*, 2007, **107**, 4891–4932.
25 O. Altan Bozdemir, S. Erbas-Cakmak, O. O. Ekiz, A. Dana and E. U. Akkaya, *Angew. Chem., Int. Ed.*, 2011, **50**, 10907–10912.
26 K. Xu, Y. Xie, X. Cui, J. Zhao and K. D. Glusac, *J. Phys. Chem. B*, 2015, **119**, 4175–4187.
27 C. Zhang, J. Zhao, S. Wu, Z. Wang, W. Wu, J. Ma, S. Guo and L. Huang, *J. Am. Chem. Soc.*, 2013, **135**, 10566–10578.
28 J. Zhao, W. Wu, J. Sun and S. Guo, *Chem. Soc. Rev.*, 2013, **42**, 5323–5351.
29 C. Zhang and J. Zhao, *J. Mater. Chem. C*, 2016, **4**, 1623–1632.
30 J. Zhao, S. Ji and H. Guo, *RSC Adv.*, 2011, **1**, 937–950.
31 H. Imahori, M. E. El-khouly, M. Fujitsuka, O. Ito, Y. Sakata and S. Fukuzumi, *J. Phys. Chem. A*, 2001, **105**, 325–332.
32 W. Qin, M. Baruah, M. Van Der Auweraer, F. C. De Schryver and N. Boens, *J. Phys. Chem. A*, 2005, **109**, 7371–7384.
33 F. Santoro, V. Barone, T. Gustavsson and R. Improta, *J. Am. Chem. Soc.*, 2006, **128**, 16312–16322.
34 T. Asahi, M. Ohkohchi, R. Matsusaka, N. Mataga, R. P. Zhang, A. Osuka and K. Maruyama, *J. Am. Chem. Soc.*, 1993, **115**, 5665–5674.
35 H. Guo, Q. Li, L. Ma and J. Zhao, *J. Mater. Chem.*, 2012, **22**, 15757.
36 S. Vyas and P. K. Sharma, *J. Chem. Sci.*, 2002, **114**, 137–148.
37 S. Feskov, V. Gladkikh and A. I. Burshtein, *Chem. Phys. Lett.*, 2007, **447**, 162–167.
38 O. Holtomo, M. Nsangou, J. J. Fifen and O. Motapon, *J. Mol. Model.*, 2014, **20**, 2509.
39 C. Fehling and G. Friedrichs, *J. Am. Chem. Soc.*, 2011, **133**, 17912–17922.
40 K. Yokoyama, Y. Wakikawa, T. Miura, J. I. Fujimori, F. Ito and T. Ikoma, *J. Phys. Chem. B*, 2015, **119**, 15901–15908.
41 Y. Wang, S. Zhang, S. M. Sun, K. Liu and B. Zhang, *Chin. J. Chem. Phys.*, 2013, **26**, 651–655.
42 X. Liu, L. Chen, Q. Zhou, X. Zhou and S. Liu, *J. Photochem. Photobiol., A*, 2013, **269**, 42–48.
43 L. Chen, Q. Zhou, X. Liu, X. Zhou and S. Liu, *Chin. J. Chem. Phys.*, 2015, **28**, 493–500.
44 A. Yu, K. Lin, X. Zhou, H. Wang, S. Liu and X. Ma, *J. Phys. Chem. C*, 2007, **111**, 8971–8978.
45 L. Chen, W. Zhu, K. Lin, N. Hu, Y. Yu, X. Zhou, L. F. Yuan, S. M. Hu and Y. Luo, *J. Phys. Chem. A*, 2015, **119**, 3209–3217.
46 M. Frisch, G. W. Trucks, H. B. Schlegel, G. E. Scuseria, M. A. Robb, J. R. Cheeseman, G. Scalmani, V. Barone, B. Mennucci and G. A. Petersson, *Gaussian 09*, Gaussian. Inc., Wallingford, CT, 2009.
47 Y. Y. Cheng, T. Khoury, R. G. C. R. Clady, M. J. Y. Tayebjee, N. J. Ekins-Daukes, M. J. Crossley and T. W. Schmidt, *Phys. Chem. Chem. Phys.*, 2010, **12**, 66–71.
48 W. Wu, H. Guo, W. Wu, S. Ji and J. Zhao, *J. Org. Chem.*, 2011, **76**, 7056–7064.
49 V. Gray, D. Dzebo, A. Lundin, J. Alborzpour, M. Abrahamsson, B. Albinsson and K. M. Poulsen, *J. Mater. Chem. C*, 2015, **3**, 11111–11121.
50 T. W. Schmidt and F. N. Castellano, *J. Phys. Chem. Lett.*, 2014, **5**, 4062–4072.